



Zbik, Marek and Frost, Ray L. (2009) *Micro-structure differences in kaolinite suspensions*.  
*Journal of Colloid and Interface Science*, 339(1). pp. 110-116.

© Copyright 2009 Elsevier

1                                   **Micro-Structure Differences in Kaolinite Suspensions**

2  
3                                   **Marek S. Żbik, Ray L. Frost**

4  
5                                   School of Physical and Chemical Sciences, Queensland University of Technology 2 George Street,  
6                                   GPO Box 2434, Brisbane Qld 4001 Australia.

7  
8  
9                                   **Corresponding Author:**

10  
11                                   **Ray L. Frost**

12                                   **P: +61 7 3138 2407**

13                                   **F: +61 7 3138 1804**

14                                   **E: [r.frost@qut.edu.au](mailto:r.frost@qut.edu.au)**

# Micro-Structure Differences in the Kaolinite Suspensions

Marek S. Żbik, Ray L. Frost

School of Physical and Chemical Sciences, Queensland University of Technology 2 George Street,  
GPO Box 2434, Brisbane Qld 4001 Australia.

## Abstract

SEM observations of the aqueous suspensions of kaolinite from Birdwood (South Australia) and Georgia (USA) show noticeable differences in physical behaviour which has been explained by different microstructure constitution. Birdwood kaolinite dispersion gels are observed at very low solid loadings in comparison with Georgia KGa-1 kaolinite dispersions which remain fluid at higher solids loading. To explain this behaviour, the specific particle interactions of Birdwood kaolinite, different from interaction in Georgia kaolinite have been proposed. These interactions may be brought about by the presence of nano-bubbles on clay crystal edges and may force clay particles to aggregate by bubble coalescence. This explains the predominance of stair step edge-edge like (EE) contacts in suspension of Birdwood kaolinite. Such EE linked particles build long strings that form a spacious cell structure. Hydrocarbon contamination of colloidal kaolinite particles and low aspect ratio are discussed as possible explanations of this unusual behaviour of Birdwood kaolinite. In Georgia KGa-1 kaolinite dispersions instead of EE contact between platelets displayed in Birdwood kaolinite, most particles have edge to face (EF) contacts building a cardhouse structure. Such an arrangement is much less voluminous in comparison with the Birdwood kaolinite cellular honeycomb structure observed previously in smectite aqueous suspensions. Such structural characteristics of KGa-1 kaolinite particles enable higher solid volume fractions pulps to form before significantly networked gel consistency is attained.

**Key words:** clay aggregates, kaolinite microstructure, Georgia Kaolinite, Birdwood Kaolinite, colloids, clay gelation

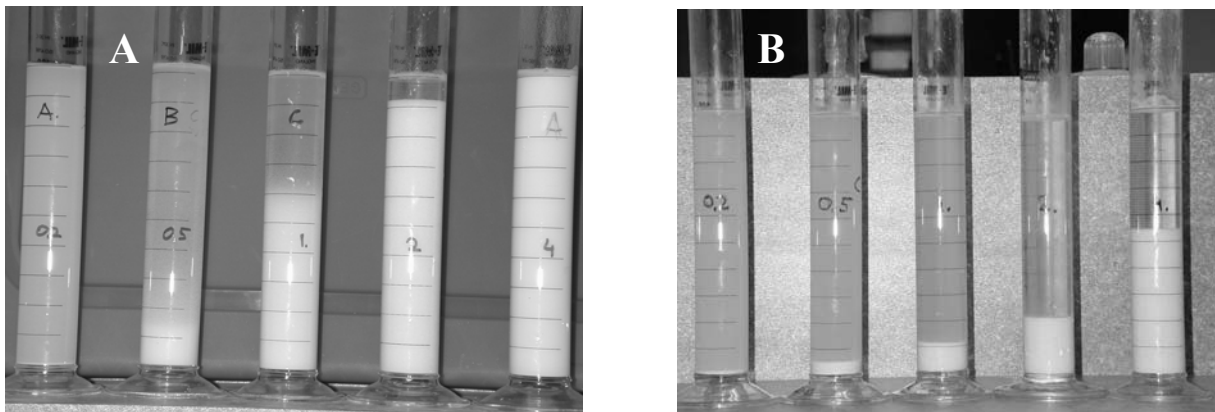
46 **Introduction**

47

48 All contemporary approaches for controlling clay suspension behaviour are based on the theory  
49 of colloid stability developed by Derjaguin and Landau [1], and Verwey and Overbeek [2]. This  
50 theory, known as DLVO theory, is where competing repulsive electrostatic and attractive van der  
51 Waals forces determine if a particular colloid clay suspension will be stable (in sol form) or  
52 coagulate (in gel form). On the basis of DLVO theory Hogg [3] described opportunities for the  
53 control of floc characteristics by physical displacement between particles, chemical changes in pore  
54 electrolyte, and introduction of a new mineral phase into the system. All these manipulations may  
55 collapse the electrical double layer, which will lower the electrokinetic potential that may bring  
56 particles close enough to allow the Van der Waals forces to bond particles into larger aggregates  
57 and significantly speed up the sedimentation rate.

58

59



60

61 **Fig. 1 Bench test of different concentration of solids in (A) Birdwood kaolinite and (B)**  
62 **Georgia kaolinite suspensions in the pH 8.**

63

64 However not all kaolinite suspensions produce sols which display DLVO behaviour, and  
65 some of them, like kaolinite from Birdwood in South Australia [4], show unusual behaviour and gel  
66 at very low solid loadings. Similar behaviour was reported in suspensions of natural oil-containing  
67 kaolinite from Canada [5] and Australian kaolinite associated with coal deposits [6] which was  
68 recognised as the major cause of difficulties in flocculating these suspensions.

69

70 An example how differently kaolinites may behave in aqueous suspension is shown in the bench  
71 test Fig. 1. This tests presented shows differences in the settling behaviour between Birdwood (A)

72 and Georgia KGa-1 (B) kaolinite suspensions which differ in solids loading (from left to the right,  
73 0.2 wt%, 0.5 wt%, 1 wt%, 2 wt%, and 4 wt%). At a very low loading content (0.2 wt%) particles in  
74 both kaolinites are well disperse and only larger crystals settled to the bottom of the cylinder. When  
75 solid content is increased (0.5 wt% and 1 wt%) a gelling mass forms at the bottom of the cylinders  
76 with some particles remaining dispersed in the suspension above the gelling mass. Gelling is more  
77 advanced in the case of Birdwood kaolinite (Fig. 1A) When solids concentration exceeds a certain  
78 value the suspension gels and locks large and minute particles in a three-dimensional network  
79 leaving clear supernatant above the compacting gel (2 wt%). Inside the gelled part of suspension  
80 free settling is not observed but more or less restricted hindered compaction takes place. Denser  
81 suspensions (4 wt%) are very slowly to compact and in case of the Birdwood kaolinite the gelled  
82 sample resists to settle.

83

84 In the references [5, 6] it has been suggest that particles in such gels are in constant contact  
85 with each other by creating a three-dimensional structure. Such a structure was also reported in the  
86 first ever SEM observations of the clay particle in dilute suspensions [6] where kaolinite platelets  
87 were found to form contacts with surrounding particles in a three-dimensional network. In this  
88 work, dilute suspensions of two different kaolinites microstructural properties were investigated  
89 with focus on particle mutual arrangements. These mutual particles arrangements create aggregate  
90 3-D microstructure which is responsible for suspension macroscopical behaviour. Present  
91 investigation will test this hypothetical statement.

92

## 93 **Experimental**

94

95 The material used for this study was commercially available K15GM kaolinite from Birdwood in  
96 South Australia [4] and Georgia kaolinite, KGa-1. The latter was obtained from the Clay Minerals  
97 Society; and is a fully characterised sample [7].

98

99 Dry kaolinite was mixed with aqueous  $10^{-2}$  M NaCl electrolyte at high solid content by shaking  
100 in a SPEX mill for 5 min. The slurries were then diluted to the required solid concentrations (4  
101 wt.%) and stirred for 2 h using a magnetic stirrer.

102

103 For the microstructural studies of the suspensions, cryo-transfer method of sample preparation  
104 was used [8] to avoid structural rearrangement caused by surface tension during oven or room

105 temperature drying. The vitrified samples were kept in a frozen state and placed onto the liquid  
106 nitrogen cooled specimen stage of the Philips XL30 Field Emission Gun Scanning Electron  
107 Microscope with Oxford CT 1500HF Cryo-stage. The samples were fractured under vacuum and  
108 sublimated after which they were coated with gold and palladium to a thickness of 3 nm. The  
109 samples were then examined in the SEM using a cathode voltage of 5 kV.

110

111 A transmission X-ray microscope with 60 nm tomographic resolution has been installed at  
112 beamline BL01B[2] of NSRRC in Taiwan. This device has a superconducting wavelength shifter  
113 source, which provides a photon flux of  $5 \times 10^{12}$  photons/s/0.1 % bw in the energy range 5-20  
114 keV. X-rays generated by a wavelength shifter are primarily focused at the charge coupled detector  
115 by a toroidal focusing mirror with focal ratio nearly 1:1. A double crystal monochromator  
116 exploiting a pair of Ge (111) crystals selects X-rays of energy 8-11 keV. After passing through the  
117 focusing mirror and double crystal monochromator, the X-rays are further shaped by a capillary  
118 condenser. Its entrance aperture is about 300  $\mu\text{m}$ , with an end opening about 200  $\mu\text{m}$  and is 15 cm  
119 long. This capillary condenser gives a reflection angle of 0.5 mrad with respect to the propagation  
120 direction. The condenser intercepts the impinging X-rays and further focuses them onto the sample  
121 with a focusing efficiency as high as 90% due to the totally reflecting nature inside the capillary.  
122 The zone-plate is a circular diffraction grating consisting of alternating opaque and transparent  
123 concentric zones. In the microscope, the zone-plate is being used as an objective lens magnifying  
124 the images  $44 \times$  and  $132 \times$  for the first order and third order diffraction mode, respectively.  
125 Conjugated with a  $20 \times$  downstream optical magnification, the microscope provides total  
126 magnification of  $880 \times$  and  $2640 \times$  for first order and third diffraction order mode, respectively. The  
127 phase term can be retrieved using the Zernike's phase contrast method that was introduced in light  
128 microscopy since the 1930s. The gold-made phase ring positioned at the back focal plane of the  
129 objective zone-plate retards or advances the phase of the zeroth- order diffraction by  $\pi/2$ , resulting  
130 in a recording of the phase contrast images at the detector.

131

132 Electrokinetic potential in both samples was measured in function of pH using AcoustoSizer II  
133 (colloidal Dynamics) in 0.01 M NaCl in 6 wt % kaolinite suspensions and particle size distribution  
134 was determined from Mastersizer (Malvern Instrument) apparatus.

135

136

137

138

139 **Results and discussions**

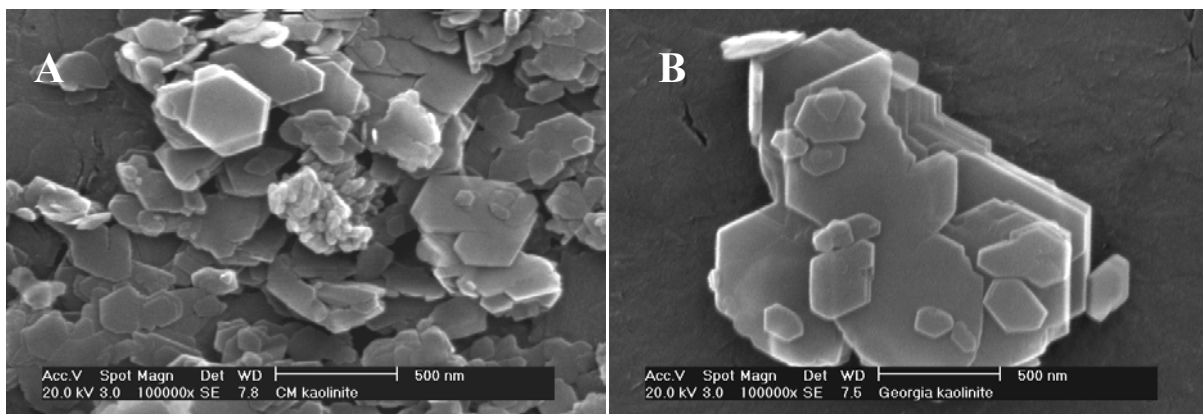
140

141 The grain size investigation show that both kaolinities are similar in dispersion, however the  
142 specific surface area found by N<sub>2</sub> –BET was 19.7 m<sup>2</sup>/g in case of Birdwood kaolinite [9] and 15.3  
143 m<sup>2</sup>/g in case of Georgia kaolinite [7] suggesting that the Birdwood kaolinite contained slightly finer  
144 particles.

145

146 Differences in the sedimentation behaviour between the kaolinite samples were displayed and  
147 were most probably caused by differences in particle electrostatic charge and morphology as well  
148 as the texture pattern when networking in a three-dimensional structure. Consequently the  
149 morphology of kaolinite samples was studied using SEM (Fig. 2).

150



151

152 Fig. 2 High resolution SEM images of (A)- Birdwood kaolinite finest colloidal fraction, (B)-  
153 Georgia KGa-1 kaolinite finest colloidal fraction.

154

155

156 The colloidal fraction of Birdwood kaolinite consists of pseudo hexagonal euhedral crystals  
157 with dimensions down to ~50 nm (Fig. 2A). The crystals typically are thin and flexible plates of  
158 very high aspect ratio (ratio of average diameter to platelet thickness is above 12). SEM  
159 investigations of fine (below 2 μm) fraction of Birdwood kaolinite show that crystals are on  
160 average 160 nm in diameter (150 particles measured) and about 13 nm thick. SEM micrographs of  
161 the Georgia KGa-1 kaolinite (Fig. 2B) also show pseudo hexagonal euhedral crystals but the  
162 platelets in KGa-1 kaolinite appear to be thicker, more rigid and better crystalline than in Birdwood  
163 kaolinite. The aspect ratio of Birdwood kaolinite is therefore higher than for Georgia kaolinite  
164 which was described in [10] and estimated as 5.3 in average.

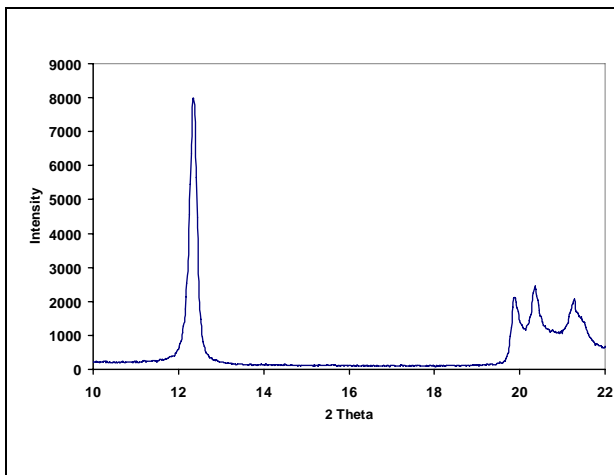


Fig. 3a XRD pattern of low and high pH Georgia Kaolinite GKa-1, powder sample, randomly oriented, sample recorded using Cu K\_ radiation.

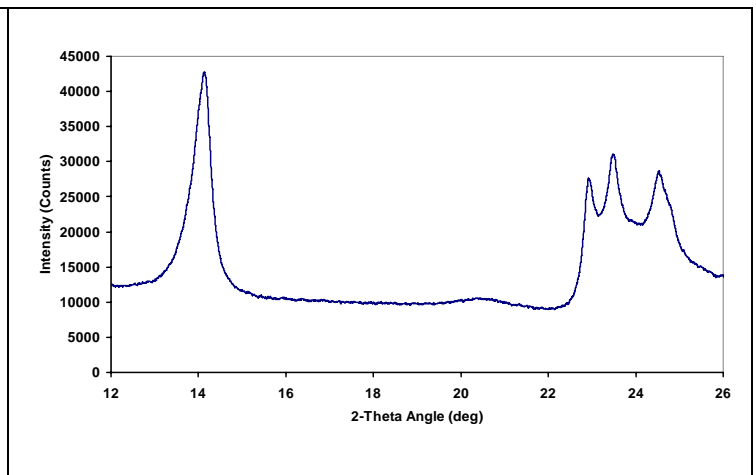


Fig 3b XRD pattern of powder sample recorded using Co K\_ radiation.

165

166

167

168

169

170

171

172

173

174

175

176

177

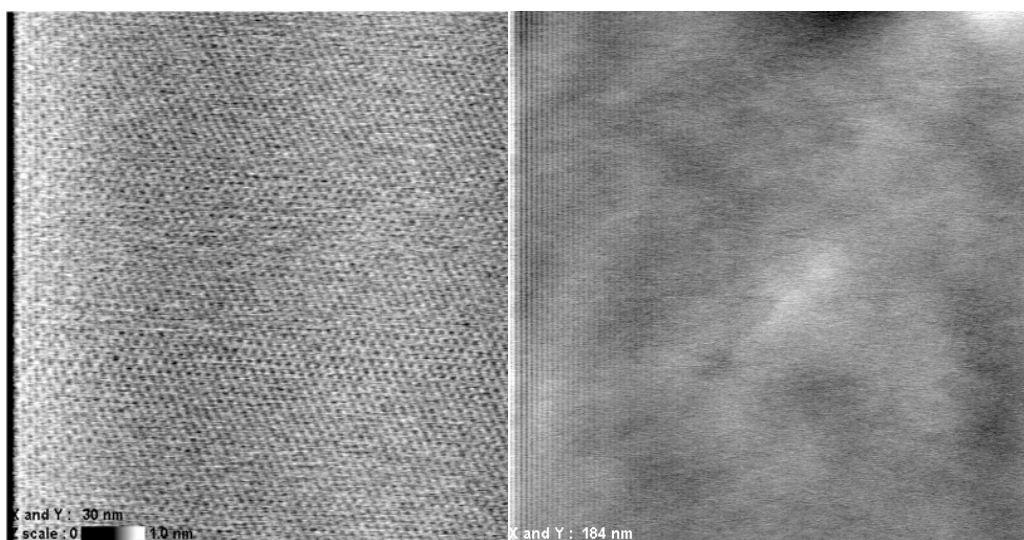
178

179

180

181

The XRD pattern (Fig. 3) and other characterisations of the KGa-1b kaolinite from Georgia (USA) have been extensively studied and well-described, described in [5]. XRD of Birdwood kaolinite described in [7] displays medium crystallinity (Hinckley index 0.75) with a broad X-ray peak centred at 3.8 Å indicating that an amorphous compound may be present. A few grape shaped anatase aggregates and a few tubular halloysite particles were also observed. The amorphous material reported in [4] can occasionally be seen in SEM and AFM images. Such colloids have never been observed in the micrographs from KGa-1 Georgia kaolinite (Fig. 2B). XRD of Georgia kaolinite proved to be better crystalline than the Birdwood kaolinite (Hinckley index 0.99). X-ray diffraction pattern of the Birdwood kaolinite has been discussed in [4] and shows a strong asymmetry on the low angle side of the 0 0 1 peak. It is suggested that interstratified smectite-like layers may be present in this kaolinite [11]. XRD of Birdwood kaolinite also displays poorly crystalline kaolinite with a broad X-ray peak indicating that an amorphous compound may be present.



182

183

184 **Fig 4 The high resolution AFM micrographs of the KGa-1 (left, frame is 30 nm) and**  
185 **Birdwood kaolinite (right, frame is 184 nm).**

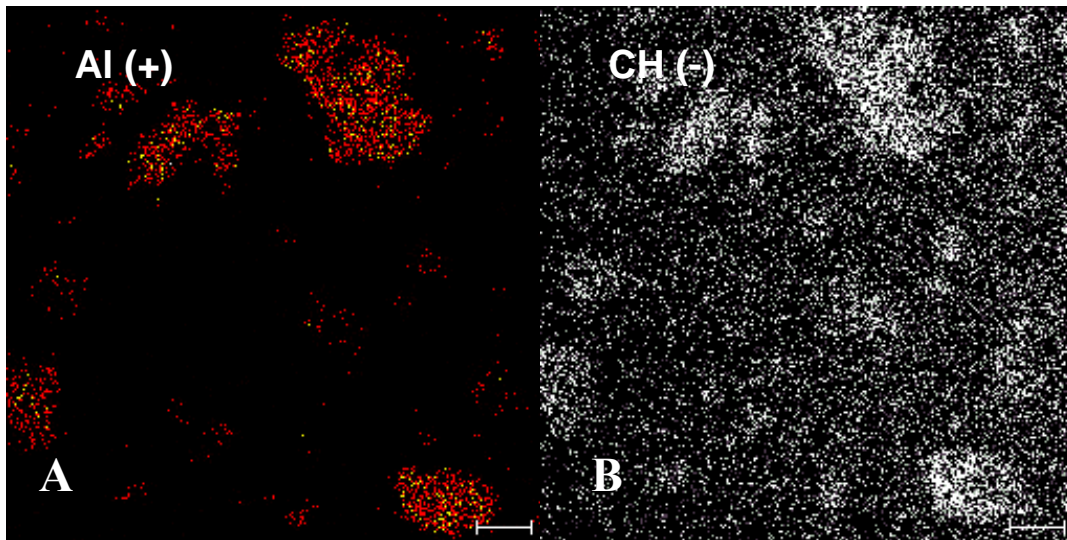
186

187 The AFM investigations of surface morphology of both kaolinites are presented in Fig 4 shown  
188 that KGa-1 kaolinite display clean surface where molecular arrangements of oxygen atoms in  
189 siloxane layer is clearly visible. In contrary at the surface of the Birdwood kaolinite crystal features  
190 are not visible which may be interpreted that surface in this kaolinite is rough and contaminated.

191

192 To check possible contamination Birdwood kaolinite was also studied by time of flight  
193 secondary mass spectrometry (ToFSIMS) and confirmed hydrocarbon component on top of  
194 kaolinite platelets (Fig. 5). Unfortunately it is not possible to determine how the hydrocarbon is  
195 distributed across individual kaolinite crystals faces. Some evidence for this contention has been  
196 seen in imaging of species on the aggregate surfaces. There is a clear association of CH<sup>-</sup> fragment  
197 images with both Al<sup>+</sup> and Si<sup>+</sup> images possibly suggesting partially hydrophobic species but there is  
198 no evidence of any effect of these species on the electrokinetic behaviour of the kaolinite and  
199 carbonaceous contamination of surfaces is well known to be ubiquitous. If present, however, even  
200 in small concentrations, surfactants would also help to explain the stability of the micro bubbles  
201 and even gaseous film in the mineral interfaces detailed described recently in [12]. Georgia  
202 Kaolinite KGa-1 has not been investigated in ToFSIMS technique.

203



204

205

206 **Fig. 5 TOF-SIMCE images of colloidal Birdwood kaolinite deposit on silicon wafer (scale bare**  
 207 **10  $\mu\text{m}$ ). Selected positive Aluminium ions (A) and negative ion images (B). Please note**  
 208 **that the CH (-3) represents HC (hydrocarbons).**

209

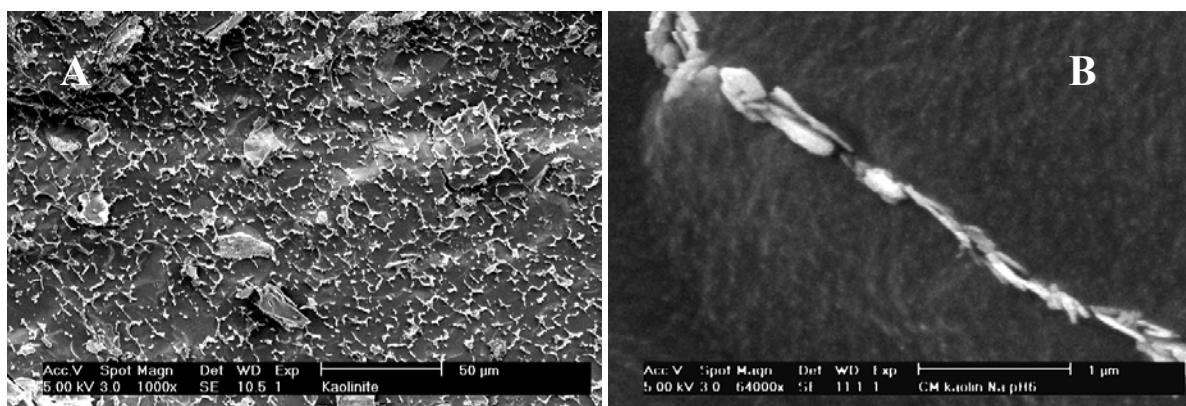
210 The grain size measurements in studied Birdwood bulk kaolin sample show that 10% of  
 211 particles have diameters smaller than 0.52  $\mu\text{m}$ , 50% of particles have diameters smaller than 4.62  
 212  $\mu\text{m}$  and 90% of particles have diameters smaller than 20.6  $\mu\text{m}$  and a specific surface area  $19.7 \pm 0.5$   
 213  $\text{m}^2\text{g}^{-1}$  (BET).

214

215 The Birdwood kaolinite when investigated using cryo-SEM techniques revealed edge to edge  
 216 (EE) particle orientation (Fig. 6). Electron microscopy observation of the clay suspension structure  
 217 shows discrete particles link together forming a coagulated spanned network (Fig. 6A) that extends  
 218 throughout all the suspension via clay platelets networking (EE) orientation. This structure is  
 219 similar to cellular honeycomb types described before in [13]. These chain-aggregates are few  $\mu\text{m}$   
 220 long and encircling large voids filled with electrolyte 1-10  $\mu\text{m}$  in diameter. These highly porous  
 221 super-structure build of elongated aggregates and chain associations have been described before in  
 222 [9, 11, 12, 13] as a flocculated but dispersed structure. Such gel structured suspensions are typical  
 223 of those observed in Birdwood kaolinite by SEM [9] are difficult to explain on the basis of DLVO  
 224 theory because positively charged edges should repel each other. Furthermore, the van der Waals  
 225 forces, which are the normal cause of coagulation, does not favour (EE) contacts because these  
 226 would have weaker attraction than edge-to-face (EF) or face-to-face (FF) contacts.

227

228 In the high resolution cryo-SEM micrograph (Fig. 6B) however more complex particle  
229 arrangement is revealed. Colloidal in size kaolinite platelets build string like aggregate (wall of  
230 cellular structural element) but their connection is not exactly edge to edge (EE) but rather in sort  
231 of stairs-step arrangement where following platelet covers in FF arrangement, fraction of preceded  
232 particle surface. This arrangement can be only observed in the high resolution images and in lower  
233 resolution imaging it is seen as EE contact. Also platelets in such aggregates are not separate  
234 crystal in the thickness but few platelets connected in the FF arrangement with hand of card like  
235 shifted on edges. This arrangement looks suits stair step connection between aggregates and forms  
236 this long stringy like aggregate which builds the cellular structure walls.  
237



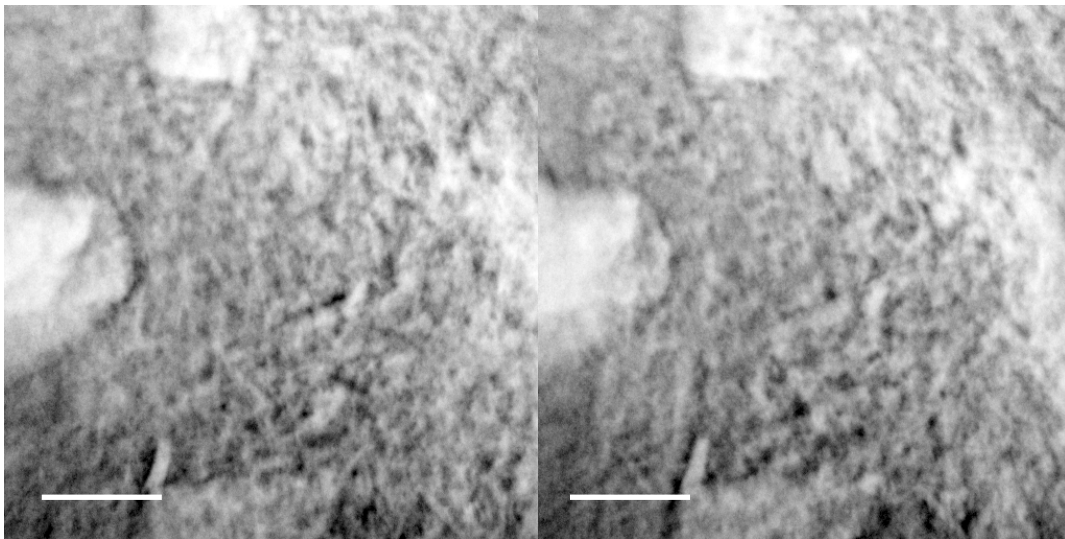
238  
239  
240 **Fig. 6 Cryo-SEM micrographs of the Birdwood kaolinite in dilute aqueous suspension (4**  
241 **wt%) shows in low magnification micrograph (A)- cellular texture which forms the**  
242 **spanned network of gelled particles in mostly edge to edge platelets and chains**  
243 **orientation, and in high resolution micrograph (B)- details of particle connection**  
244 **within chained aggregate discussed in text.**

245  
246 As an explanation of the predominance of such contacts it is proposed in [13] that hydrophobic  
247 like attraction between aerated edges may occur and platelets may rolling on top of each other with  
248 help of air micro-bubbles well described in [12]. Such mostly EE linked particles build long strings  
249 seen in two dimensional SEM images as sections of planar structure that connect to each other to  
250 build a spacious cell structure as shown in Fig 4B.

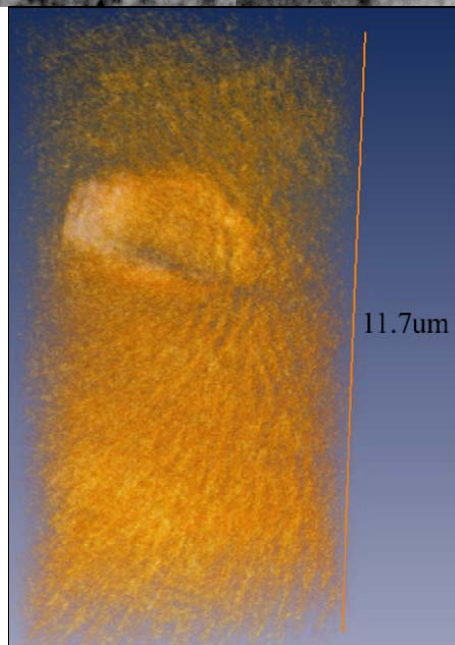
251  
252 In the TXM stereo pare micrographs from of the 8 wt% Birdwood kaolin water suspension as  
253 shown in Fig. 7, the long chained aggregates consisted of numerous colloidal size platelets like  
254 described above in cryo-SEM investigations. These elongated chains like aggregates have been

255 denser packed in chaotic network in which even larger grains are immobilised. The long chained  
256 aggregates in this micrograph are well wrapped with other similar and heavily cross linked.  
257 Cellular like voids in these micrographs are usually below 1  $\mu\text{m}$  in diameter. Some illusion of high  
258 packing in these micrographs can be explained by long focal length of TXM images. The long focal  
259 length (50  $\mu\text{m}$ ) makes many particles in thicker suspension being viewed simultaneously in focus  
260 which in effect will obscure some particles and may have negative impact on image clarity.

261



262



263

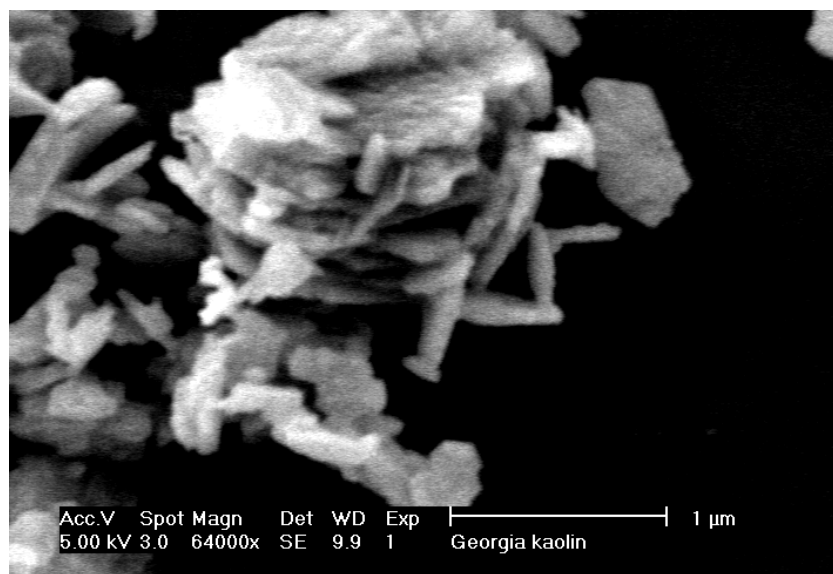
264

265 **Fig. 7 TXM stereo pares micrograph (top) from water suspension in 8 wt% of Birdwood**  
266 **kaolin. Scale bar is 2.5  $\mu\text{m}$ . (Bottom) - Snapshot from 3-D reconstruction of a**  
267 **Birdwood kaolinite suspension. Larger stacked crystals are entangled in the network**  
268 **of colloidal kaolinite platelets, characteristic string like network pattern can be**  
269 **observed.**

270

271 This snapshot of 3-D stereo pares from TXM in a Birdwood kaolinite suspension demonstrated  
272 in Fig. 7 show a dense network of colloidal kaolinite particles supports a larger kaolinite stacked  
273 crystal of few  $\mu\text{m}$  in lateral dimension. This micrographs may be not giving very impressive picture  
274 as compared with other well established techniques such as SEM, but enable us to examine clay  
275 aggregates in 3-D through water, which has never been previously possible. Individual colloidal  
276 size particles are visible in this picture magnification and distinctive string-like spongy and highly  
277 oriented structure is observable when carefully studying this micrograph under stereoscope or in 3-  
278 D computer reconstruction shown in [18].

279



280

281 **Fig. 8 SEM micrographs of the Georgia KGa-1 kaolinite micrograph show mostly edge to**  
282 **face (EF) platelet orientation.**

283

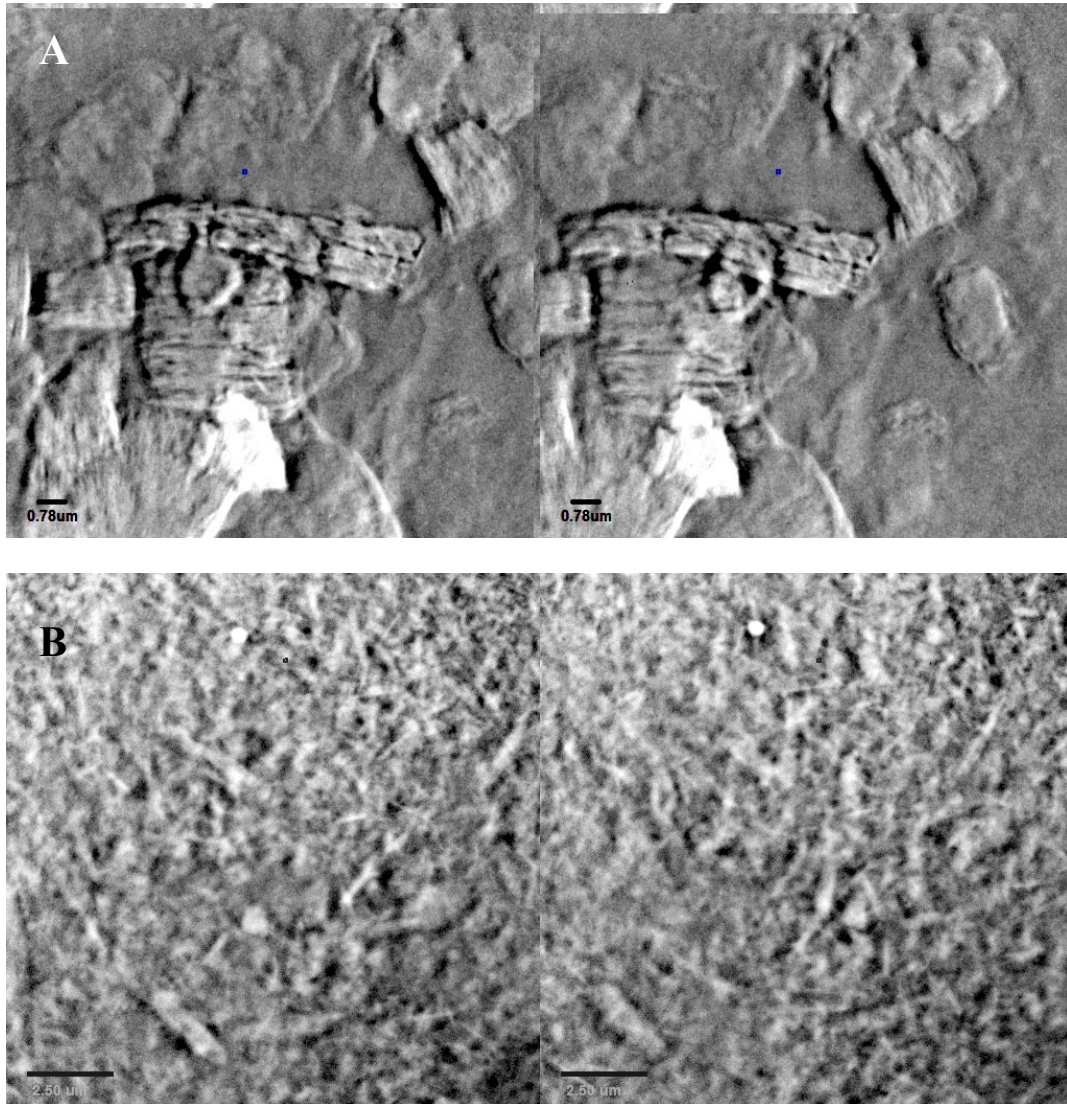
284 Studied KGa-1 kaolinite sample consists of two morphologically distinctive kaolinite  
285 populations, fine to colloidal kaolinite platelets and larger stacked crystals. Ninety percent by  
286 weight of the particles have an equivalent spherical diameter less than  $2 \mu\text{m}$  with a median particle  
287 size of  $0.7 \mu\text{m}$  and a specific surface area of  $15.3 \pm 0.5 \text{ m}^2\text{g}^{-1}$  (BET). The fine kaolinite fraction in  
288 SEM investigations using the cryo-transfer technique (Fig. 6) show a very different particle  
289 arrangement than observed in Birdwood kaolinite suspensions. Instead of EE contact arrangement  
290 between platelets as in Birdwood kaolinite, in KGa-1 kaolinite most particles have edge to face  
291 (EF) contacts. Such an arrangement is much less voluminous in comparison to the Birdwood

292 kaolinite suspension structure and particles in the networked flocs of KGa-1 are much closer  
293 together.

294

295

296



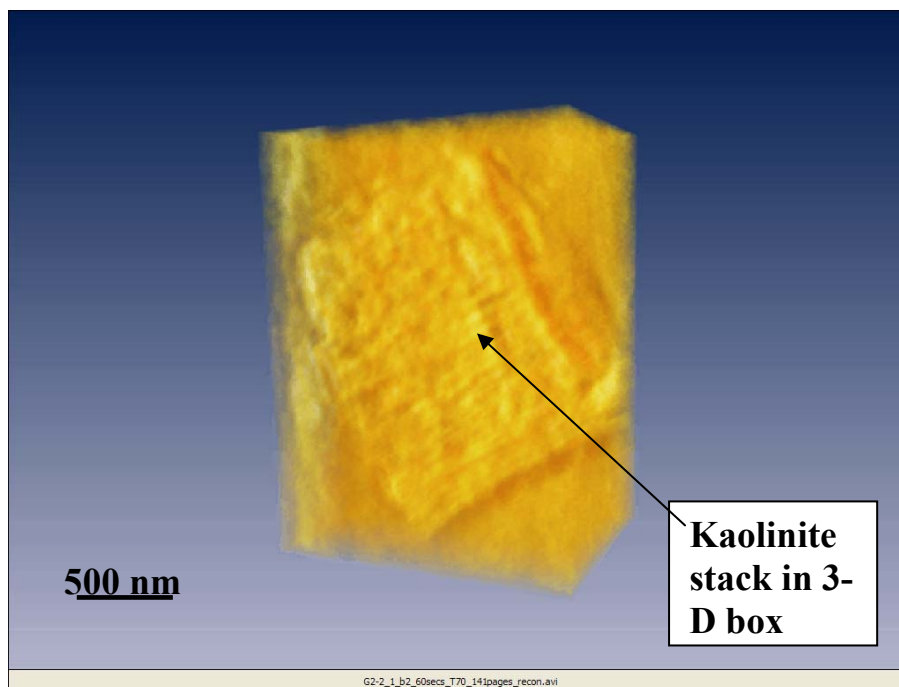
297  
298

299  
300  
301  
302  
303  
304

**Fig. 9 TXM stereoscopic pares from KGa-1 kaolinite sample in water suspension show: (A) flock of stacked kaolinite crystals (scale bar 780 nm) and (B) mostly EF connected fine kaolinite platelets (scale bar 2.5 μm).**

305 In sample (KGa-1) a few μm in dimension stacked kaolinite crystals, are more common than in  
306 the Birdwood kaolinite where stacks are less common and they are smaller in dimension. **In Fig. 10**  
307 two 2-D TXM micrographs of KGa-1 kaolinite shot from different angles (stereo pares) reveal  
308 aggregates consisting of randomly connected stacked kaolinite crystals 2–4 μm in dimension.  
309 Stacks show distinctive lamination 150 nm thick and randomly contact each other through rugged  
310 edges. Individual platelets up to 2 μm in diameter were observed. The aqueous solution  
311 surrounding these kaolinite stacks shows distinctive gaps between the water and solid surface at  
312 several places as well as apparent voids within aggregates. This type of gaseous bubbles and film

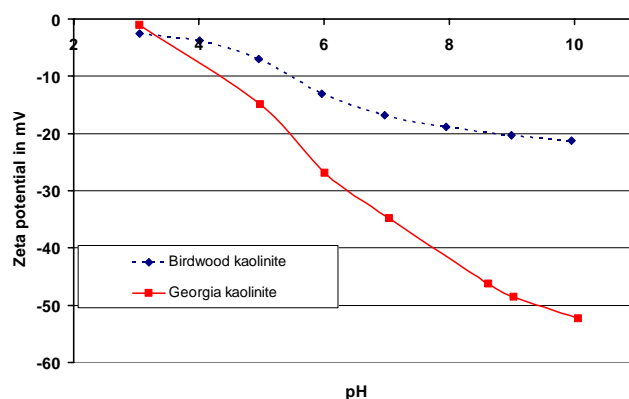
313 presence was detailed described in [12] where cryo-SEM investigations revealed that water not  
314 wetting mineral surface leaving gaseous film on the solid/liquid interface. The gaps adjacent to the  
315 mineral surface are 80–100 nm thick and appear to continuously cover substantial parts of the  
316 aggregate surfaces. This gaseous gap may be because of hydrophobic interaction between siloxane  
317 layer of kaolinite crystals and water. Such a gaseous blanketing at the mineral interface can be  
318 eliminated by ultrasonic treatment [12]. Hydrophobic interaction between clay particles surrounded  
319 in such blankets was nominated as the major factor in aggregation and structure building in [14].  
320 Hydrocarbon contamination was suspected the effect of such hydrophobic interaction in Birdwood  
321 kaolinite. However TXM observations recorded possible gaseous films associated with larger  
322 stacks in KGa-1 kaolinite. Such nano-bubbles occurrence in area of rough edges (which are  
323 common in kaolinite stacks) and in puckering between siloxane layers in talk which was described  
324 in [15 and 16]. This wetting phenomenon is very complex and includes mineral/water interface  
325 chemistry, contamination and morphology in nano-scale.



326  
327 **Fig 10 3-D reconstruction of the Kaolinite stack from coarse fraction of Georgia kaolinite**  
328 **sample as seen within the aqueous solution. Stacking is visible as well as fine fraction of**  
329 **kaolinite particles adhered towards stack edges which are more clearly visible when picture is**  
330 **rotated. Dimension of cube is  $\sim 2 \times 4 \mu\text{m}$ .**

331  
332 In the TXM stereo pares show in Fig. 7B the colloidal fraction of kaolinite sample KGa-1 in  
333 density 8 wt% is presented in 3-D space arrangement. This stereo pares as well as computer 3-D

334 reconstruction (not shown here) show dense suspension with particles in face to edge arrangement  
335 with most voids below 0.5  $\mu\text{m}$ .



336

337 **Fig. 11 Zeta potential of Birdwood and Georgia (KGa-1) kaolinite suspensions measured on**  
338 **AcoustoSizer.**

339

340 The electrokinetic (zeta) potential measured for both kaolinite samples shown in **Fig. 11**  
341 displays major differences. The KGa-1 kaolinite sample displays typical pH-dependent profile due  
342 to  $\text{OH}^-$  groups occupied platelets edges in high pH. The Birdwood kaolinite displays smectite like,  
343 very low pH-dependence suggesting dominance of the basal plane. Such dominance may be due to  
344 blockage of particle edges by colloids, hydrocarbons and possible gaseous phase associated with  
345 colloidal hydrocarbon contamination. Such blockage of the edge sites may significantly reduce  
346 repulsive forces between particle edges and in consequence system will favourite the EE particle  
347 arrangement.

348 Within the context of the microscopical observations shown in Fig. 1 may be interpreted as  
349 follows: At low solids loading, separate particles and particle aggregates are suspended in the water  
350 solution and settle freely accordingly to the Stokes' law. When solid loading increases it reaches a  
351 critical particle concentration at which closest particles interact and start to form a three-  
352 dimensional structure. In the case of Birdwood kaolinite individual particles interact by attracting  
353 each other towards their edges and build an extremely large voluminous network composed of  
354 chain-like platelet assemblages. Such an extended network may fill the entire volume of a vessel.  
355 In such a case the suspension is gelled; there is no free settling in this system and compacting  
356 occurs slowly by structure recombination. The process of Birdwood kaolinite sludge recombination  
357 is described in detail in [9]. The settling velocity of thick sludges is presented also [17].

358 Kaolinite from Georgia (KGa-1) forms more compact aggregates by preferring edge to wall  
359 orientation and as result forms a less porous network than Birdwood kaolinite. This means that for  
360 KGa-1 kaolinite to build a gel suspension for which the gel spans the entire volume of the vessel  
361 requires a much greater solids loading than for Birdwood kaolinite (Fig. 1).

362 Described above differences in gelling properties in studied two kaolinite samples explained  
363 here by mayor differences in way like individual particles are connected in to tree-dimensional  
364 network may have its cause in differences in studied minerals the aspect ratio. This difference in  
365 the aspect ratio may effects in physical properties such as the lower dependability of the zeta  
366 potential in changing pH, rougher edges, and higher aspect ratio observed in Birdwood kaolinite  
367 which effects in the highly porous arrangement of individual particles in the three-dimensional  
368 network. But the mechanism influenced these differences is still obscure and need further  
369 investigations.

370

## 371 **Conclusions**

372

373 Within the context of structural differences of clay-water suspensions using the cryo-SEM and  
374 the synchrotron based TXM with 3-D reconstruction, observed in Fig. 1 behaviours can be  
375 interpreted as follows. At low solids loading, separate particles and particle aggregates are  
376 suspended in the water solution and settle freely governed by the Stokes' law. When solid loading  
377 increases it reaches a critical particle concentration at which closest particles interact and start to  
378 form a three-dimensional structure. In the case of Birdwood kaolinite individual particles interact  
379 by attracting each other towards their edges by stair step elongated aggregates and build an  
380 extremely large voluminous smectite like cellular, honeycomb type structure previously reported in  
381 [13]. Such extended network may fill the entire volume of a vessel. In such a case, the suspension  
382 is gelled; there is no free settling in this system and compaction occurs slowly by structure re-  
383 arrangement. The process of Birdwood kaolinite sludge recombination is described in detail in [9].  
384 Because aggregates which form in the Birdwood kaolinite suspension are very long, they attracted  
385 in network building phenomenon other similar aggregates from much larger distances than  
386 dimension of single platelets. Three dimensional network build of such aggregates is extremely  
387 voluminous and suspension gels in relatively low solid content.

388 It is possible that hydrophobic interaction between kaolinite particles plays important role in  
389 structure making process. Possible hydrocarbon contamination at the mineral interface shown in

390 Birdwood kaolinite may contribute to formation gaseous microbubbles. However such film of  
391 gasses also was observed in TXM images of Georgia kaolinite interpreted as hydrophobic  
392 repelling of water by non wetted siloxane tetrahedral layer. Nature of this phenomenon is obscure  
393 and need further investigations.

394 Kaolinite from Georgia (KGa-1) forms compact aggregates by preferring edge to face  
395 orientations. Electrostatic interaction between particle edges and faces build network with voids  
396 diameter corresponds to particles dimensions. As the result, sediment bead is packed much denser  
397 than in Birdwood kaolinite. This means that for KGa-1 kaolinite to build a gel suspension for which  
398 the gel spans the entire volume of the vessel requires a much greater solids loading.

399 Observed differences in gelling properties in the two kaolinite samples may be explained in  
400 terms of major differences in particle surface chemistry and aspect ratio. These properties in the  
401 kaolinite mineral structure and possible smectite like interstratifications may effect in physical  
402 properties such as the lower zeta potential on basal surfaces, rougher face surfaces, and higher  
403 aspect ratio observed in Birdwood kaolinite which effects in the highly porous arrangement of  
404 individual particles in the three-dimensional network. But the mechanism influenced these  
405 differences is still obscure and need further investigations.

406

407 **References:**

408

409 [1] B. V. Derjaguin, L. D. Landau, *Acta Physicochim. URSS.*, **14**, (1941) 633-652.

410 [2] W. Verwey, J. Th. G. Overbeek, *The theory of Stability of Lyophobic Colloids*, Elsevier,  
411 Amsterdam, Netherlands, (1948).

412 [3] R. Hogg, *Int. J. Miner. Process.* **58**, (2000) 223-236.

413 [4] R.L. Frost, S.J. Van Der Gaast, M. Zbik, J.T. Kloprogge, G.N. Paroz, *App. Clay Science.* **20**,  
414 (2002) 177-187.

415 [5] L.S. Kotlyar, B.D. Sparks, Y. LePage, J.R. *Clay Minerals* **33**, (1998) 103-107.

416 [6] N.R. O'Brien, *J. of Electron Microscopy* **19**, (1970) 277.

417 [7] S.J. Chipera, D.L. Bish, *Clays and Clay Minerals.* **49** No. 5, (2001) 398-409.

418 [8] P. Smart, N.K. Tovey, *Electron microscopy of soils and sediments: technique.* (1982)  
419 Clarendon Press, Oxford.

420 [9] M.S. Zbik, R.St.C. Smart, G.E. Morris, (2008), *J. Colloid Interface Sci.* **328**, (2008) 73-80

421

422 [10] M. Zbik, R.St.C. Smart, *Proc. 11<sup>th</sup> Int. Clay Conf, Ottawa, 15-21 June 1997*, Ottawa, Canada,  
423 (1999) 361-366.

424 [11] H. Van Olphen, *An introduction to clay colloid chemistry:* (1963) New York, Wiley.

425 [12] M.S. Zbik, Jianhua Du, Rada A. Pushkarova, R.St.C. Smart, (2009) *J. Colloid Interface Sci.*  
426 **336**, 616-623

427 [13] R.H. Bennet, M.H. Hulbert, *Clay Microstructure*, IHRDC, (1986) Boston, Houston, London.

428 [14] M. Zbik, R.G. Horn. *Coll. & Surf. A:* **222**, (2003) 323-328.

429 [15] M. Zbik, R.St.C. Smart, *Min. Engin.*, **15**, (2002) 277-286.

430 [16] W. Gong, J. Stearnes, D. Fornasiero, R.A. Hayes, J. Ralston, *J. Phys. Chem. Chem. Phys.* **1**,  
431 (1999) 2799-2803.

432 [17] Cheremisinoff N.P. (2000) *Handbook of Water and Wastewater Treatment Technologies.*  
433 Butterworth Heinemann. Boston Oxford Auckland Johannesburg Melbourne New Delhi, 282-  
434 284.

435 [18] M.S. Zbik, R. L. Frost, Y-F. Song. (2008) *J. Colloid Interface Sci.* **319**, 169-174

436

437 ***List of Figures***

438

439 **Fig. 1 Bench test of different concentration of solids in (A) Birdwood kaolinite and (B)**  
440 **Georgia kaolinite suspensions in the pH 8.**

441 **Fig. 2 High resolution SEM images of (A) Birdwood kaolinite finest colloidal fraction, (B)**  
442 **Georgia KGa-1 kaolinite finest colloidal fraction.**

443 Fig. 3a XRD pattern of low and high pH Georgia Kaolinite GKa-1, powder sample, randomly  
444 oriented, sample (a) recorded using Cu K<sub>α</sub> radiation (b) XRD pattern of powder sample recorded  
445 using Co K<sub>α</sub> radiation.

446

447 Fig 4 The high resolution AFM micrographs of the KGa-1 (left, frame is 30 nm) and Birdwood  
448 kaolinite (right, frame is 184 nm).

449

450 **Fig. 5 TOF-SIMCE images of colloidal Birdwood kaolinite deposit on silicon wafer (scale bare**  
451 **10 μm). Selected positive Aluminium ions (A) and negative ion images (B). Please note that**  
452 **the CH (-3) represents HC (hydrocarbons).**

453 **Fig. 6 Cryo-SEM micrographs of the Birdwood kaolinite in dilute aqueous suspension (4**  
454 **wt%) shows in low magnification micrograph (A)- cellular texture which forms the spanned**  
455 **network of gelled particles in mostly edge to edge platelets and chains orientation, and in high**  
456 **resolution micrograph (B)- details of particle connection within chained aggregate discussed**  
457 **in text.**

458 **Fig. 7 TXM stereo pares micrograph from water suspension in 8 wt% of Birdwood kaolin.**  
459 **Scale bar is 2.5 μm.**

460

461 **Fig. 8 SEM micrographs of the Georgia KGa-1 kaolinite micrograph show mostly edge to**  
462 **face (EF) platelet orientation.**

463 **Fig. 9 TXM stereoscopic pares from KGa-1 kaolinite sample in water suspension show: (A)**  
464 **flock of stacked kaolinite crystals (scale bar 780 nm) and (B) mostly EF connected fine**  
465 **kaolinite platelets (scale bar 2.5 μm).**

466

467 **Fig 10 3-D reconstruction of the Kaolinite stack from coarse fraction of Georgia kaolinite**  
468 **sample as seen within the aqueous solution. Stacking is visible as well as fine fraction of**

469 **kaolinite particles adhered towards stack edges which are more clearly visible when picture is**  
470 **rotated. Dimension of cube is  $\sim 2 \times 4 \mu\text{m}$ .**

471

472 **Fig. 11 Zeta potential of Birdwood and Georgia (KGa-1) kaolinite suspensions measured on**  
473 **AcoustoSizer.**

474

475